BNL-211218-2019-TECH
NSLSII-ASD-TN-286

Longitudinal Beam Dynamics with a Higher-Harmonic Cavity for Bunch Lengthening

G. Bassi

September 2018

Photon Sciences
Brookhaven National Laboratory

U.S. Department of Energy
USDOE Office of Science (SC), Basic Energy Sciences (BES) (SC-22)

DISCLAIMER

NSLS II TECHNICAL NOTE BROOKHAVEN NATIONAL LABORATORY	NUMBER NSLSII-ASD-TN-286
AUTHOR G. Bassi, J. Tagger	DATE 9/30/2018
TITLE Longitudinal Beam Dynamics with a Higher-Harmonic Cavity for Bunch Lengthening	

Longitudinal Beam Dynamics with a Higher-Harmonic Cavity for Bunch Lengthening

G. Bassi and J. Tagger
Brookhaven National Laboratory, Upton, NY 11973, USA

Introduction

Higher-harmonic cavities (HHCs) play a crucial role for stable operations of present and future low-emittance storage rings. The primary benefic effect provided by the HHC is bunch lengthening without energy spread increase, with consequent beam lifetime improvement and reduction of the effect of intrabeam scattering on the transverse emittance [2]. Besides bunch lengthening, the highly nonlinear potential well distortion produced by the HHC introduces a strong dependence of the synchrotron tune on the amplitude of synchrotron oscillations. The induced anharmonic motion with enhanced synchrotron tune spread provides a powerful mechanism, known as Landau damping, for the suppression of collective instabilities. Moreover, the increase in bunch length and synchrotron tune spread can enhance the stabilizing effect of positive chromaticity on the transverse oscillations and help to stabilize higher-order head-tail modes [2]. The option considered for the NSLS-II storage ring is to operate with a passive superconducting 3HC [3], [4], [5], a choice supported by the successful development and operation of the superconducting 3HC system at the ELETTRA [6] and SLS [7] storage rings, a system that has been developed in the framework of the SUPER-3HC project [8]. The SUPER-3HC project represented the first superconducting application of a HHC system in storage rings, taking advantage of the very high quality factor of the superconducting cavity and the associated narrow bandwidth, allowing for the tuning of the 3HC very near to the third harmonic of the beam, without exciting longitudinal instabilities [6]. The success of the 3HC operation at the ELETTRA storage ring is substantiated by a beam lifetime improvement by more than a factor of three with respect to the nominal value, an improvement that has led to a change in the refilling frequency of the storage ring, allowing a refilling every 48hr instead of every 24hr, with benefit for the reliability and stability of user's operations and relevant benefit even for the machine thermal stability [6]. The success with the operation of a 3HC at the SLS storage ring is substantiated by a bunch lengthening up to a factor of three and a beam lifetime increase greater than a factor of two, achieved with stable conditions at the design current of 400 mA [7].
The success experienced at the ELETTRA and SLS storage rings has clearly shown that the very high quality factor of the superconducting HHC renders the performance of the HHC system less sensitive to high-order modes (HOMs) driven longitudinal coupled bunch instabilities, which is a major issue with normal conducting HHCs, where powerful longitudinal feedback systems are often needed for stable

operations. Performance limiting factors, however, such as transients effects induced by non uniform filling patterns and the beam phase instability [9], can be detrimental for stable HHC operations, and need to be carefully investigated with detailed design studies, a need that is justified also by the fact that stable conditions of operation are often very sensitive to the machine parameters.

Accurate numerical simulations represent an essential part of the aforementioned design studies, with their goal to determine feasible conditions of operation and their range of applicability. To this end, the stability and performance of the passive superconducting 3HC system for the NSLSI-II storage ring is studied numerically with the parallel, particle tracking code SPACE [10], which allows to follow self-consistently the dynamics of h bunches, where h in the number of RF buckets, each with a distinct bunch population. The specific goal of the numerical simulations is to determine stable HHC cavity settings and to study the performance limitation due to a gap in the uniform filling, which represent the nominal NSLS-II mode of operation.

The paper is organized as follows. In Sect.1 we review the conditions of operation of an HHC system assuming its stability. We first discuss the longitudinal dynamics with an active HHC and the conditions that lead to a quartic potential in the limit of small oscillations, together with formulae giving the bunch lengthening factor and the synchrotron frequency dependence on the amplitude of the synchrotron oscillations. We discuss next passive HHC operations with uniform fillings, and distinguish the case of normal-conducting HHC, where optimal conditions of operation can be met, from the case of superconducting HHC, where optimal conditions of operation can be satisfied only approximately. In Sect.2 we address the stability of the passive superconducting 3HC system of the NSLS-II storage ring via self-consistent simulations with code SPACE. The case of nominal fractional filling of 80% is compared with the case of fractional filling of 90% and with the uniform filling case. It is shown that for values of the detuning frequency in the neighborhood of the good working point discussed in Sect.2, unstable regimes of oscillation are found, with detuning frequency threshold dependent on the gap in the filling. It is shown that the instability regime is characterized by dipole and quadrupole modes of oscillation exhibiting asymptotically nonlinear saturation. A discussion of the average bunch lengthening, together with the degree of uniformity across the bunch train, achievable under stable conditions as a function of the fractional filling concludes the paper.

1 Operations with Higher-Harmonic Cavities

In the discussion of the theoretical conditions for optimal bunch lengthening, we assume a stable, beam loading compensated HHC system characterized by an equilibrium multi-bunch configuration. Radiation damping and quantum fluctuations are excluded from the analysis. The overall stability of the HHC system, including radiation damping and quantum fluctuations, together with the inclusion of a model for beam loading compensation, will be addressed in Sec.IV with time dependent simulations of the Vlasov-Fokker-Planck equation.

1.1 Active Higher-Harmonic Cavity

We assume that the voltage $V(\tau)$ seen by a particle in the beam with arrival time τ is

$$V(\tau) = V_{rf}[\sin(\omega_{rf}\tau + \phi_s) - r\sin(m\omega_{rf}\tau + \phi_m)] - \frac{U_0}{e} =: V_c(\tau) - \frac{U_0}{e}, \tag{1}$$

where V_{rf} is the amplitude of the voltage of the main RF cavity, $\omega_{rf} = h\omega_0$, where h is harmonic number and ω_0 the angular revolution frequency, m is the order of the HHC and r the ratio of HHC to main cavity amplitude voltage, U_0 energy loss per turn, e the electron charge, ϕ_s and ϕ_m the phases of the synchronous particle in the main and HHC respectively. Here $V_c(\tau)$ is the total RF voltage produced by the main RF cavity and HHC.

Parameter	Symbol	Value	Unit
Energy reference particle	E_0	3	GeV
Average current	I_0	500	mA
Gap in the uniform filling	g	260	
Harmonic number	h	1320	
Circumference	C	792	m
Bunch duration	σ_τ	14.5	ps
Energy spread	σ_p	0.00087	
Energy loss per turn	U_0	674	keV
Momentum compaction	α	0.00037	
Revolution frequency	f_0	378.5	kHz

Table 1: NSLSII storage ring parameters

RF parameters main cavity system (2 cavities)

Per Cavity Parameters	Symbol	Value	Unit
Frequency	ω_{rf}	$2\pi\times499.68$	MHz
Voltage	V_{rf}	1.7	MV
Loaded shunt impedance	R_M	2.97	MΩ
Loaded quality factor	Q_M	66817	

RF parameters HHC system (1 cavity)

Per Cavity Parameters	Symbol	Value	Unit
Frequency	$m\omega_{rf}$	$2\pi\times1499.04$	MHz
Shunt impedance	R_H	22880	MΩ
Quality factor	Q_H	2.6×10^8	

Table 2: RF parameters main and HHC (m=3)

The longitudinal dynamics in the double RF system described by Eq.(1) has been comprehensively discussed, together with optimal conditions for bunch lengthening, by Hofmann and S. Myers in 1980 [13]. See also [15]. Here we summarize the main results.
To compensate for the energy loss U_0, we require that the voltage seen by the synchronous particle is zero, i.e. $V(0)=0$. In addition, we require $V'(0)=V''(0)=0$, where $'=d/d\tau$. These conditions imply

$$\sin\phi_s = r\sin\phi_m + \frac{U_0}{eV_{rf}}, \tag{2}$$

$$\cos\phi_s = rm\cos\phi_m, \tag{3}$$

$$\sin\phi_s = rm^2\sin\phi_m, \tag{4}$$

which, solved for ϕ_s, ϕ_m and r give

$$\sin\phi_s = \frac{m^2}{m^2-1}\sin\phi_{s0}, \quad \sin\phi_{s0} = \frac{U_0}{eV_{rf}}, \tag{5}$$

$$\tan\phi_m = \frac{m\sin\phi_{s0}}{\sqrt{(m^2-1)^2 - m^4\sin^2\phi_{s0}}}, \tag{6}$$

$$r = \frac{1}{m}\sqrt{1-\frac{m^2}{m^2-1}\sin^2\phi_{s0}}, \tag{7}$$

where we introduced ϕ_{s0}, the synchronous phase in absence of the HHC. With the use of Eq. (6) and Eq. (7), we notice that the voltage $V(\tau)$ can be equivalently expressed as a function of ϕ_s eliminating ϕ_m and r

$$V(\tau) = V_{rf}[\sin(\phi_s+\omega_{rf}\tau) - \sin\phi_s - \frac{\sin\phi_s}{m^2}(\cos m\omega_{rf}\tau - 1) - \frac{\cos\phi_s}{m}\sin m\omega_{rf}\tau]. \tag{8}$$

With the voltage given by Eq.(1), from the Hamiltonian

$$H(\tau,\delta) = \frac{\eta}{2}\delta^2 + U(\tau),$$
$$U(\tau) = \frac{eV_{rf}}{E_0T_0\omega_{rf}}\Big[\cos(\omega_{rf}\tau+\phi_s) - \cos\phi_s + \frac{r}{m}\cos\phi_m - \frac{r}{m}\cos(m\omega_{rf}\tau+\phi_m) + \omega_{rf}\tau\sin\phi_{s0}\Big], \tag{9}$$

follow the longitudinal equations of motion

$$\dot\tau = \frac{\partial H}{\partial\delta} = \eta\delta,$$
$$\dot\delta = -\frac{\partial H}{\partial\tau} = \frac{eV_{rf}}{E_0T_0}\Big[\sin(\omega_{rf}\tau+\phi_s) - r\sin(m\omega_{rf}\tau+\phi_m) - \sin\phi_{s0}\Big], \tag{10}$$

where $\dot{} = d/dt$, $\eta = \alpha - \gamma_0^{-2}$ is the slippage factor, where γ_0 is the Lorentz factor, $\delta = (E - E_0)/E_0$ is the relative energy deviation with respect to the synchronous particle with energy E_0, and the arbitrary constant in the definition of $U(\tau)$ has been chosen in order to satisfy $U(0) = 0$. Since U does not depend explicitly on time, H is a constant of motion and setting $E = H$ we have

$$\delta(\tau) = \pm\sqrt{\frac{2}{\eta}(E - U(\tau))}, \qquad E = \text{const.} \tag{11}$$

In Fig.1a we show the potential energy $U(\tau)$ without HHC cavity (red trace) and with HHC (blue trace) with the NSLS-II storage ring parameters (see Table 1 and 2) satisfying (5)-(7). In Fig.1b we show the corresponding phase space portrait for $E = 0.3$. With optimal conditions satisfied, the voltage $V(\tau)$ induces a bunch lengthening without an increase of the energy spread. According to Table 1 and 2, $r = 0.329 \approx 1/3$, thus the peak voltage induced by the harmonic cavity is roughly one third the peak voltage V_{rf} of the main cavity. In the case of no energy loss ($U_0 = 0$) the conditions (2)-(4) simplify to $\phi_s = \phi_m = 0$ and $r = 1/m$. In Fig.2a we plot the potential energy $U(\tau)$ for $m = 3$ and different values of r. For $r = 4/9$ the potential energy has two stable fixed points close to ± 150ps.

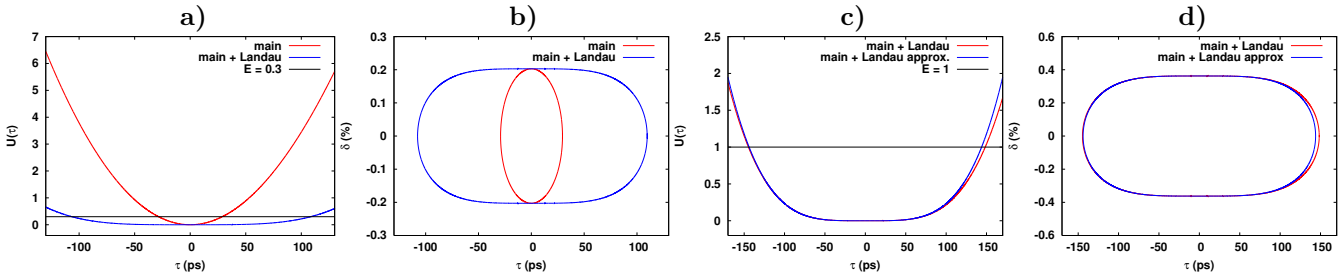

Figure 1: a) Potential energy $U(\tau)$ without HHC (red line) and with HHC (blue line) with parameters of the NSLS-II storage ring (see Table 1 and 2) satisfying Eq. (5)-(7). b) Phase space portrait corresponding to a) for $E = 0.3$. The optimal conditions satisfied by the voltage $V(\tau)$ induce a bunch lengthening without an increase of the energy spread. c) Comparison of exact and approximated results for $U(\tau)$ for the case with the HHC. d) Comparison of the phase space portraits for the case shown in c) for $E = 1$. The quartic approximation to the exact potential is quite accurate in the range $|\tau| \leq 150$ps.

1.1.1 Small Oscillations

For small oscillations ($\tau \ll 1$) the potential energy $U(\tau)$ without HHC can be approximated by a quadratic function of τ

$$U(\tau) = -\frac{eV_{rf}\omega_{rf}\cos\phi_{s0}}{2E_0T_0}\tau^2 = \frac{\omega_{s0}^2}{2\eta}\tau^2, \tag{12}$$

$$\omega_{s0} = \sqrt{-\frac{\eta eV_{rf}\omega_{rf}\cos\phi_{s0}}{E_0T_0}}, \tag{13}$$

while with the addition of the HHC the potential given by Eq.(9) can be approximated by a quartic

$$U(\tau) = -\frac{eV_{rf}(m^2-1)\omega_{rf}^3\cos\phi_s}{24E_0T_0}\tau^4. \tag{14}$$

For a potential energy satisfying $U(-\tau) = U(\tau)$ and $U(\tau) > 0$ for $\tau > 0$, the trajectory is confined in the region $[-\tau_M, \tau_M] \times [-\delta_M, \delta_M]$ where τ_M and δ_M satisfy $U(\tau_M) = E$ and $\eta\delta_M^2/2 = E$ respectively, thus the amplitude of the trajectory is $d = 2\tau_M$. In Fig.1c we compare the exact and approximated $U(\tau)$ including the harmonic cavity and in Fig.1d) we compare the corresponding phase space portrait for $E = 1$. We

see that the approximation is quite good in the range $|\tau| \leq 150$ps. It can be shown that the synchrotron frequency ω_s for the quartic potential (14) reads

$$\omega_s(\tau_M) = \frac{\pi}{2}\sqrt{\frac{m^2-1}{6}}\sqrt{\frac{\cos\phi_s}{\cos\phi_{s_0}}}\frac{\omega_{rf}\omega_{s0}}{K(1/\sqrt{2})}\tau_M, \tag{15}$$

where K is the complete integral of the first kind. The dependence of the synchrotron frequency on τ_M provides Landau damping for beam stability. In Fig.2b we plot ω_s as a function of τ_M. It can also be shown that the bunch lengthening factor u for an equilibrium distribution ρ_e in the quartic potential (14) reads

$$u := \frac{\sigma_{\tau L}}{\sigma_{\tau m}} = \Big(\frac{\Gamma(3/4)}{\Gamma(1/4)}\Big)^{1/2}\Big(\frac{24\cos\phi_{s0}}{(m^2-1)\omega_{rf}^2\cos\phi_s}\Big)^{1/4}\frac{1}{\sqrt{\sigma_{\tau m}}}, \tag{16}$$

where Γ is the Gamma function, $\sigma_{\tau_m} = \eta\sigma_\delta/\omega_{s0}$ is the equilibrium bunch length with only the main cavity, and σ_{τ_L} is the equilibrium bunch length with the harmonic cavity. The bunch lengthening factor u as a function of σ_{τ_m} is plotted in Fig.2c. For the NSLS-II parameters with $\sigma_{\tau m} = 14.5$ps we have a bunch lengthening factor $u = 3.7$.

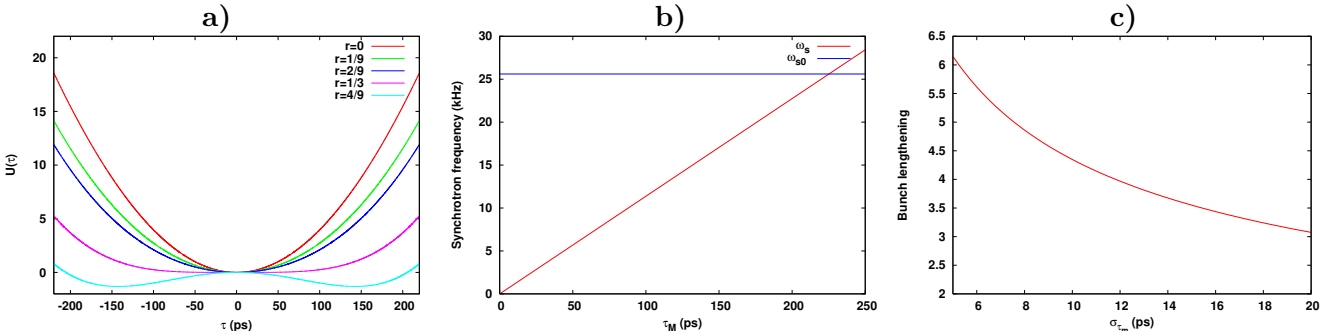

Figure 2: a) Potential energy $U(\tau)$ in the active case ($m = 3$) and for no energy loss ($U_0 = 0$). In this case the optimal conditions imply $\phi_s = \phi_m = 0$ and $r = 1/m$. Several values of r are plotted. For $r = 4/9$ the potential energy has two stable fixed points close to ± 150ps. b) Synchrotron frequency ω_s for the quartic potential (red line) and synchrotron frequency ω_{s0} for the quadratic potential (blue line). The dependence of the synchrotron frequency on the maximum amplitude τ_M provides Landau damping for beam stability. c) Bunch lengthening u vs. bunch length with main cavity alone σ_{τ_m}. For the NSLS-II parameters with $\sigma_{\tau m} = 14.5$ps the bunch lengthening is $u = 3.7$.

1.2 Passive Higher-Harmonic Cavity

For passive HHC operations, the total RF voltage is given by the sum of the voltage produced by the powered main cavity and the beam loading voltage induced by the beam in both cavities. We assume in this section that the main cavity is beam loading compensated.

1.2.1 Operations with Normal-Conducting Cavities

In the case of stationary bunches uniformly distributed around the ring, and for a narrow-band resonator wake with frequency ω_r, shunt impedance R_s and quality factor Q, the voltage acting on the beam reads

$$V_c(\tau) = V_{rf}\sin(\phi_s + \omega_{rf}\tau) - i_{im}R_s\cos\psi\cos(\psi + m\omega_{rf}\tau), \tag{17}$$

where $i_{im} = 2I_0\tilde{\rho}(\omega_r)$ and the detuning angle ψ satisfies

$$\tan\psi = 2Q\delta, \quad \delta = \frac{1}{2}\Big(\frac{\omega_r}{m\omega_{rf}} - \frac{m\omega_{rf}}{\omega_r}\Big) \approx \frac{\omega_r - m\omega_{rf}}{m\omega_{rf}}. \tag{18}$$

Here $\tilde{\rho}(\omega)$ is the Fourier transform of the bunch density $\rho(\tau)$ satisfying $\rho(-\tau) = \rho(\tau)$. For Gaussian bunches $i_{im} = 2I_0 e^{-\frac{1}{2}(m\omega_{rf}\sigma_\tau)^2}$.
Imposing the same the conditions (2)-(4) satisfied by the active HHC, by comparing (1) and (17) it follows ($0 < \phi_s < \pi \implies 0 < \psi < \pi/2 \implies \cos\psi > 0$)

$$\tan\psi = -\cot\phi_m = -m\cot\phi_s, \tag{19}$$

$$R_s = \frac{rV_{rf}}{i_{im}\cos\psi} = \frac{V_{rf}\sin\phi_s}{i_{im}m^2\cos^2\psi}, \tag{20}$$

where we used $\sin\phi_m = \cos\psi$ ($\tan\psi = -\cot\phi_m \implies \psi = \phi_m - \pi/2 \implies \sin\phi_m = \cos\psi$.) Therefore the conditions for passive HHC operations corresponding to the active case (5)-(7) are

$$\sin\phi_s = \frac{m^2}{m^2-1}\sin\phi_{s0}, \tag{21}$$

$$\tan\psi = -\frac{\sqrt{(m^2-1)^2 - m^4\sin^2\phi_{s0}}}{m\sin\phi_{s0}}, \tag{22}$$

$$R_s = \frac{V_{rf}(m^2-1)(1-\sin\phi_{s0})}{i_{im}m^2\sin\phi_{s0}}. \tag{23}$$

An important difference to the active case is that R_s is uniquely determined and a function of the beam current I_0. Notice, however, that these conditions do not impose any constraint on the value of Q, therefore do not determine uniquely the detuning frequency $\Delta\omega = \omega_r - m\omega_{rf}$.
The optimal parameters for passive HHC operations of the NSLS-II storage ring according to Table 1 and 2 are therefore

$$\begin{aligned} \sin\phi_s &= 0.4592, \\ \tan\psi &= 5.8 \implies \psi = 80.22^\circ, \\ R_s &= 9.02M\Omega. \end{aligned} \tag{24}$$

1.2.2 Operations with Super-Conducting Cavities

According to Table 2, the shunt impedance of the HHC is $R_H = 22880M\Omega$, much bigger than R_s as determined by Eq.(24), so the optimal conditions for passive operations can not be met. Good conditions, however, can be found by comparing Eq.(1) and Eq.(17) at $\tau = 0$, which gives $R_s = rV_{rf}/(i_{im}\cos\psi)$, and by noticing from Eq.(7) that $r \approx 1/m$, since to good approximation $\sin\phi_{s0}^2 \ll 1$. We therefore impose on the detuning angle ψ the condition $\cos\psi = V_{rf}/(mi_{im}R_H)$, which implies that the detuning frequency $\Delta\omega_H$ approximately satisfies

$$\Delta\omega_H = \frac{m^2\omega_{rf}i_{im}R_HV_{rf}}{2Q_HV_{rf}}, \tag{25}$$

where we used Eq.(18) and the fact that $\cos\psi \ll 1$. With parameters listed in Table 1 and 2, it follows that $\Delta\omega_H = 2\pi \times 58.24$kHz.

2 Numerical Simulations

With the inclusion of a model for beam loading compensation, time dependent simulations of the Vlasov-Fokker-Planck equation allow for the study of the overall stability of the HHC system. Moreover, numerical simulations allow for the study of transient effects induced by arbitrary multi-bunch configurations, such as a gap in the uniform filling pattern for ion clearing, which corresponds to the nominal configuration of the NSLS-II storage ring. The numerical simulations of the Vlasov-Fokker-Planck equation discussed in this

paper are done with the parallel code SPACE, a particle tracking code that allows for the simultaneous study of short- and long-range wakefield effects in storage rings. The general strategy adopted by SPACE to study multibunch effects is to distribute each bunch to one processor, each with $\mathcal{N}$ simulations particles representing the bunch population, thus performing the short- and long-range wakefield calculation in serial and parallel respectively. For more details on the code SPACE see [10]. For steady state beam loading compensation, the algorithm implemented in SPACE is based on the standard phasor diagram, shown in Fig. 3 with parameters of one of the operational settings of the NSLS-II storage ring. The numerical simulations discussed in this paper have been done on the supercomputers Cori and Edison at NERSC [14].

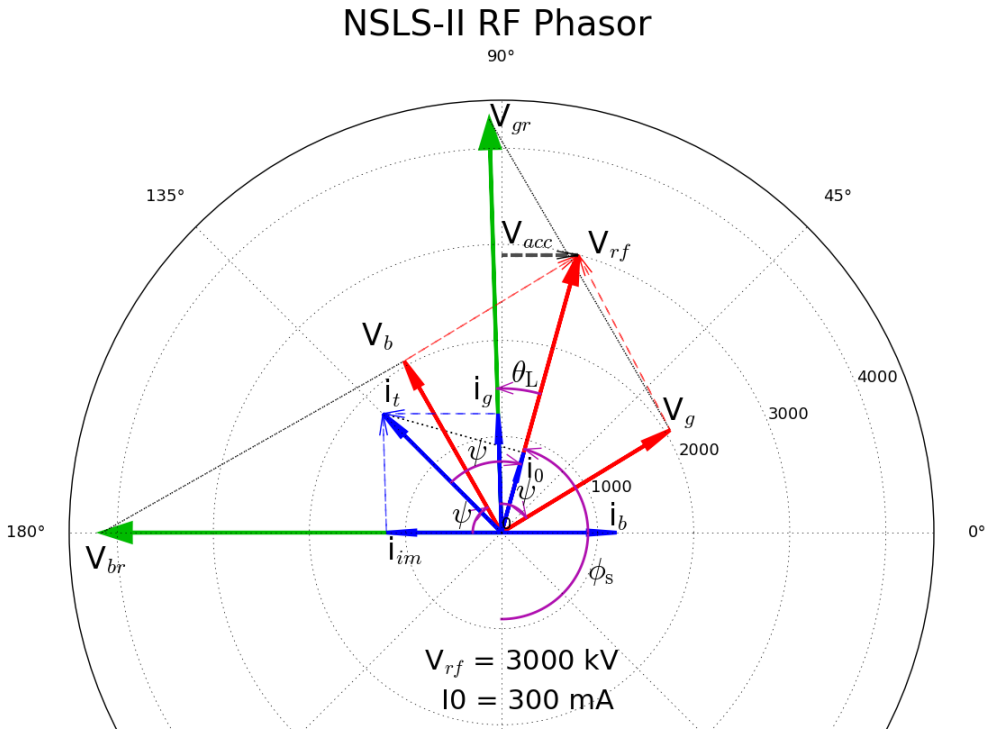

Figure 3: RF phasor of the NSLS-II storage ring during operations with a stored beam current $I_0 = 300mA$, $V_{rf} = 3000$kV, $\phi_s = 164.5°$, $\theta_L = -17°$, total forward power $P_g = 340$kW, total reflected power $P_r = 91$kW, power delivered to the beam $P_n = 240$kW, $V_b = 2062$kV, $V_g = 2132$kV, detuning angle $\psi = 60°$, $\omega_r = 2\pi \times 499.68$MHz, $\Delta\omega = \omega_r - \omega_{rf} = -5.5$kHz, $i_g = 1241$mA, $i_0 = 864$mA, $i_t = 1746$mA, energy loss per turn $U_0 = 725$keV.

The equations of motion for bunch n $(n = 0, \cdots, h-1)$, shown here without radiation damping and quantum fluctuations, for the general NSLS-II operations with two main cavities and one harmonic cavity read

$$\begin{aligned} \dot{\tau} &= \eta\delta, \\ \dot{\delta} &= \frac{e}{E_0 T_0}\Big[\sum_{i=1}^{2} V_{gr,i}\cos\Psi_i \sin(\omega_{rf}\tau + \phi_s - \theta_{L,i} + \Psi_i) - V_n(\tau, s) - \frac{U_0}{e}\Big], \end{aligned} \tag{26}$$

where $V_{gr,i}$, Ψ_i and $\theta_{L,i}$ $(i = 1, 2)$ correspond to the generator voltage, detuning angle and load angle of the two main cavities respectively, and $V_n(\tau, s)$ is the total beam loading voltage acting on bunch n. The numerical simulations discussed in this paper assume the two main cavities with same beam loading parameters, which correspond to the standard mode of operation of the NSLS-II storage ring. By projecting the current phasors shown in Fig. 3 along and perpendicular to the RF voltage phasor, V_{gr} and

Ψ satisfy

$$\tan\Psi = \Big(1 + \frac{i_{im,M}}{i_0}\sin\phi_s\Big)\tan\theta_L + \frac{i_{im,M}}{i_0}\cos\phi_s, \tag{27}$$

$$V_{gr} = \frac{V_{rf}}{\cos\theta_L}\Big(1 + \frac{i_{im,M}}{i_0}\sin\phi_s\Big), \tag{28}$$

where $i_{im,M} = 2I_0\tilde{\rho}(\omega_{rf})$ is the image current in the main cavity, and $i_0 = V_{rf}/R_M$. In the analysis of the performance of the NSLS-II HHC system, we study first the case with a uniform filling pattern, and compare the results with the nominal case, which correspond to a gap of 260 bunches, (80% fractional filling), and with the case with a gap of 130 bunches (90% fractional filling). In the discussion that follows we omit the subscript H to label the detuning frequency of the HHC.

2.1 Uniform Filling

In Fig.4 we show numerical simulations for values of the HHC detuning frequency $\Delta f = 45$kHz, 55kHz and 65kHz, above and below the value of 58.24kHz calculated in Section 1.2.2 for good bunch lengthening conditions. The longitudinal density of the bunches after $100,000$ turns is shown in Fig.4a for $\Delta f = 45$kHz, in Fig.4b for $\Delta f = 55$kHz and Fig.4c for $\Delta f = 65$kHz. The bunch lengthening is uniform across the bunch train for $\Delta f = 55$kHz and $\Delta f = 65$kHz, with values $\sigma_\tau = 50$ps and $\sigma_\tau = 36$ps respectively, as shown in Fig.4e and Fig.4f for bunch $n = 0, 260, 520, 780$ and 1039, corresponding to the bunch lengthening factors $u = 3.45$ and $u = 2.48$. For $\Delta f = 45$kHz, the longitudinal density of the bunches show a double peaked structure and a non-uniform bunch lengthening, as shown in Fig.4a and Fig.4l. Long term simulations up to $500,000$ turns, as plotted in Fig.4a and Fig.4g, show that for $\Delta f = 45$kHz the HHC system is weakly unstable, signing the transition to an "overstretching" regime, with average bunch length across the train of ≈ 70ps. The potential well of bunch $n = 0$, showing two local minima, is shown by the red trace in Fig.4n.

2.2 Gap in the Uniform Filling: $g = 130$ and $g = 260$

The case of a gap in the uniform filling corresponds to a train of $M = h - g$ bunches, where h is the harmonic number and g is the gap. The case with nominal gap, $g = 260$, corresponding to a 80% filling fraction, is compared with the case $g = 130$, corresponding to a 90% filling fraction. The main effect introduced by a gap in the uniform filling in a monotonic variation of the bunch centroid across the train, and a reduced, non uniform bunch lengthening. Fig.5 and Fig.6 show numerical simulations up to $100,000$ turns with gaps $g = 130$ and $g = 260$ respectively, for the same HHC detuning frequencies of the uniform case. The monotonic variation of the bunch centroid across the train is evident from the longitudinal density of the bunches shown in Fig.5a-c, from the time evolution of the bunch centroids shown in Fig. 5g-i, and from Fig. 5m, where it can be noticed that the range of variation of the bunch centroids increases with the decrease of the HHC detuning frequency. Fig.5d-f and Fig.5l show the non uniform bunch lengthening across the train, with a similar average value $\sigma_\tau = 35$ps for the different detuning frequencies. We notice that for $\Delta f = 45$kHz the bunches in the center of the train have longer bunch length than the bunches in the periphery of the train. The case of nominal gap, $g = 260$, is discussed in Fig.6. A detuning frequency threshold is observed in this case. For detuning frequencies above the threshold, as shown for $\Delta f = 65$kHz in Figs.6c, f and l) a stable equilibrium is reached after $100,000$ turns, with average bunch length across the train $\sigma_\tau \approx 27$ps, while for detuning frequencies below threshold, as shown in Figs.6a), d) for $\Delta f = 45$kHz and Figs.6b), e) and h) for $\Delta f = 55$kHz, an unstable regime with saturation is observed, with both the bunch lengths and bunch centroids exhibiting a well defined mode of oscillation. The numerical simulations discussed so far have been done with load angle $\theta_L = 0$. In attempt to improve stability, the two unstable configurations at the nominal gap $g = 260$ for $\Delta f = 45$kHz and 55kHz have been simulated with $\theta_L \neq 0$. The results are shown in Fig.7 for $\Delta f = 45$kHz and Fig.8 for $\Delta f = 55$kHz. In both cases we see that the

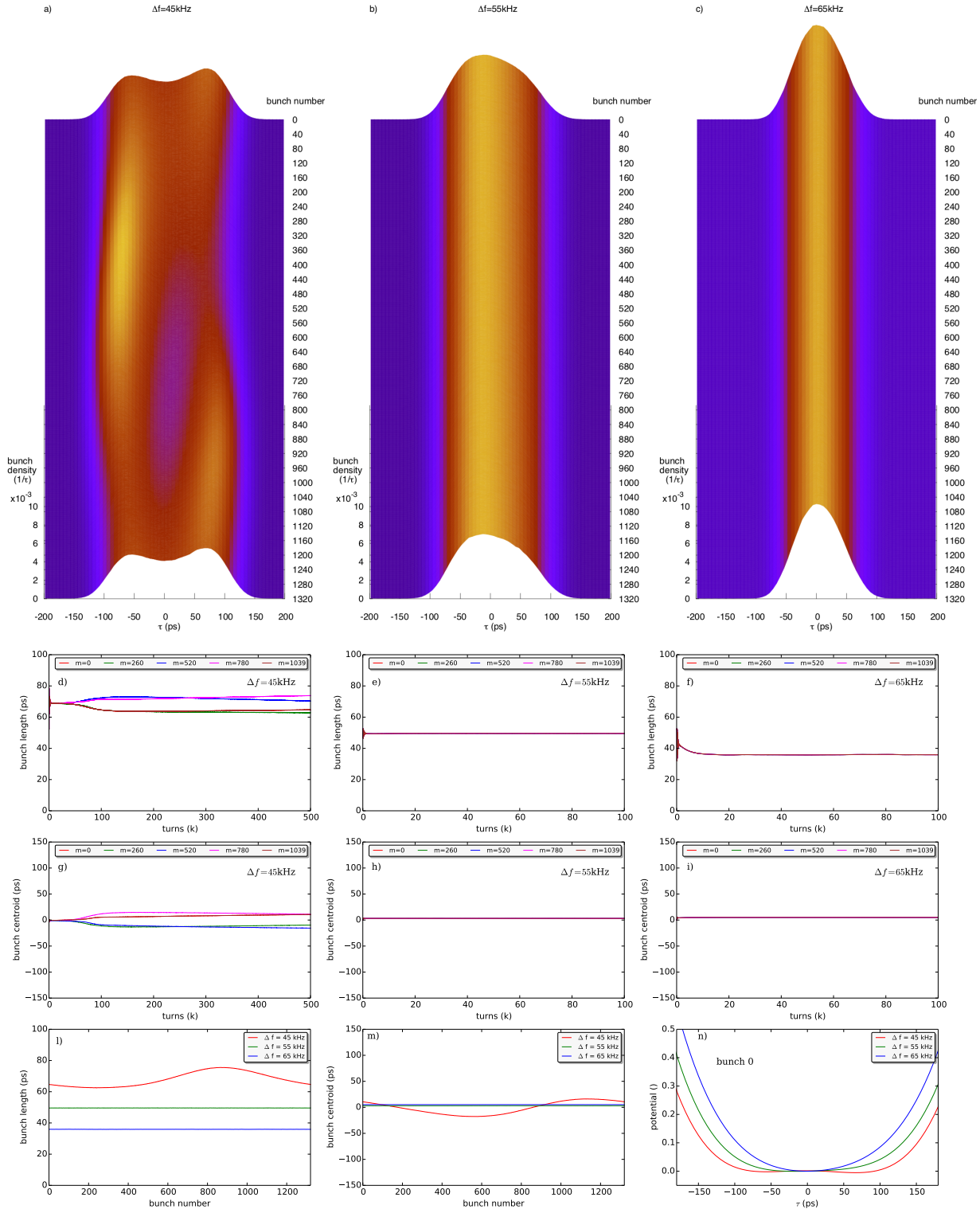

Figure 4: Numerical simulations in the case of uniform filling with detuning frequency $\Delta f = 45$kHz, 55kHz and 65kHz. Longitudinal density of the bunches after $500,000$ turns for $\Delta f = 45$kHz a), and after $100,000$ turns for $\Delta f = 55$kHz b), and for $\Delta f = 65$kHz c). The bunch lengthening is uniform across the bunch train for $\Delta f = 55$kHz e), and $\Delta f = 65$kHz f), with values $\sigma_\tau = 50$ps and $\sigma_\tau = 36$ps respectively. For $\Delta f = 45$kHz, the longitudinal density of the bunches show a double peaked structure a) and a non-uniform bunch lengthening l). g) h) and i) show the time evolution of bunch centroids, m) and n) the bunch centroids across the bunch train and potential well of bunch 0 respectively at the end of the time evolution.

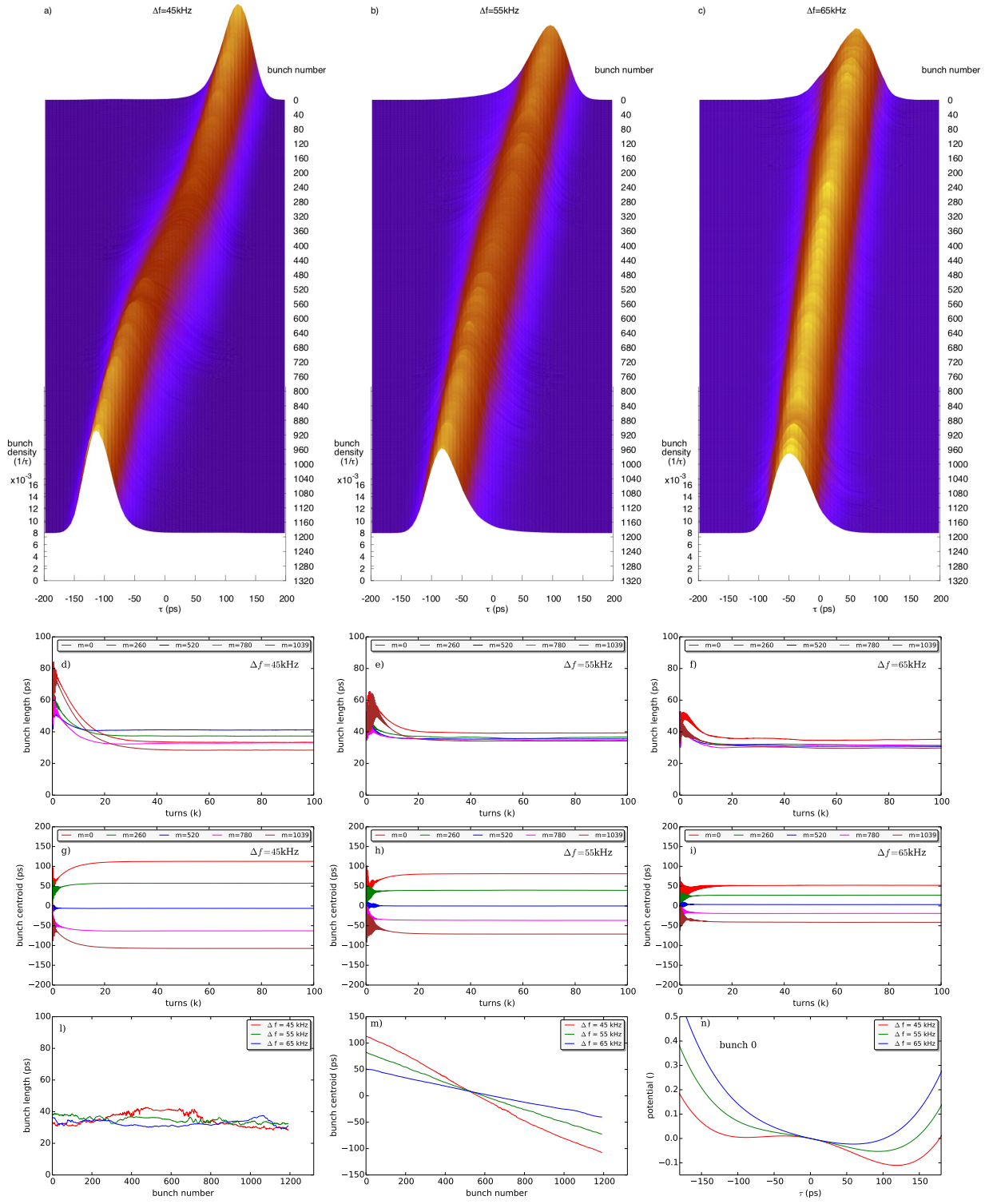

Figure 5: Numerical simulations up to 100, 000 turns with a gap $g = 130$ for the HHC detuning frequencies discussed in Fig.4. The monotonic variation of the bunch centroid across the train is evident from the longitudinal density of the bunches shown in a)-c), from the time evolution of the bunch centroids shown in g)-i), and from m), where it can be noticed that the range of variation of the bunch centroids increases with the decrease of the HHC detuning frequency. d)-f) and l) show the non uniform bunch lengthening across the train, with a similar average value $\sigma_\tau = 35$ps for the different detuning frequencies.

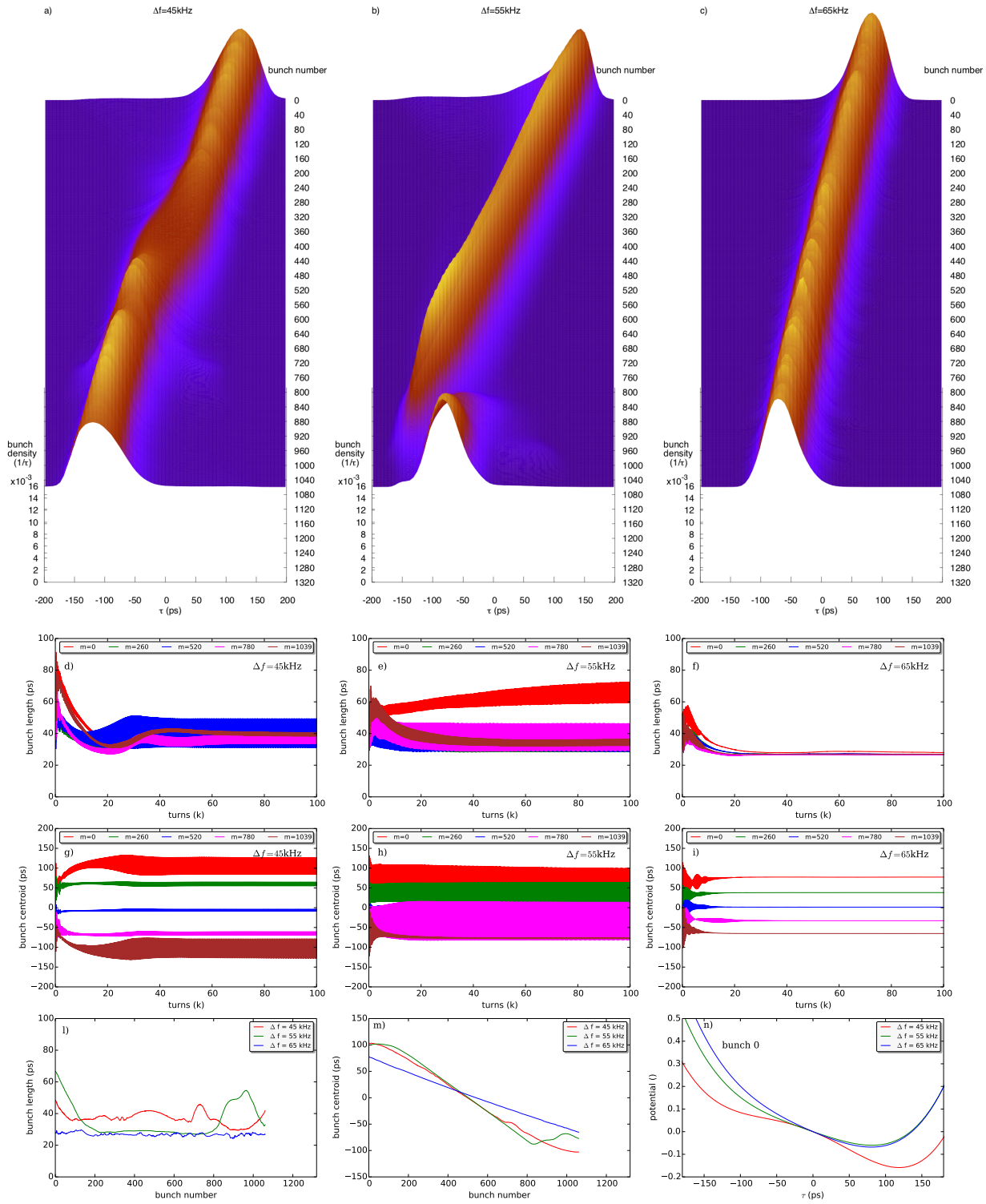

Figure 6: Numerical simulations up to $100,000$ turns with nominal gap $g = 260$, for the same HHC detuning frequencies discussed in Fig.4. A detuning frequency threshold is observed in this case. For detuning frequencies above the threshold, as shown for $\Delta f = 65$kHz in c), f) and l), a stable equilibrium is reached after $100,000$ turns, with average bunch length across the train $\sigma_\tau \approx 27$ps, while for detuning frequencies below threshold, as shown in a), d) and g) for $\Delta f = 45$kHz, and b), e) and h) for $\Delta f = 55$kHz, an unstable regime with saturation is observed, with both bunch lengths and bunch centroids exhibiting a well defined mode of oscillation.

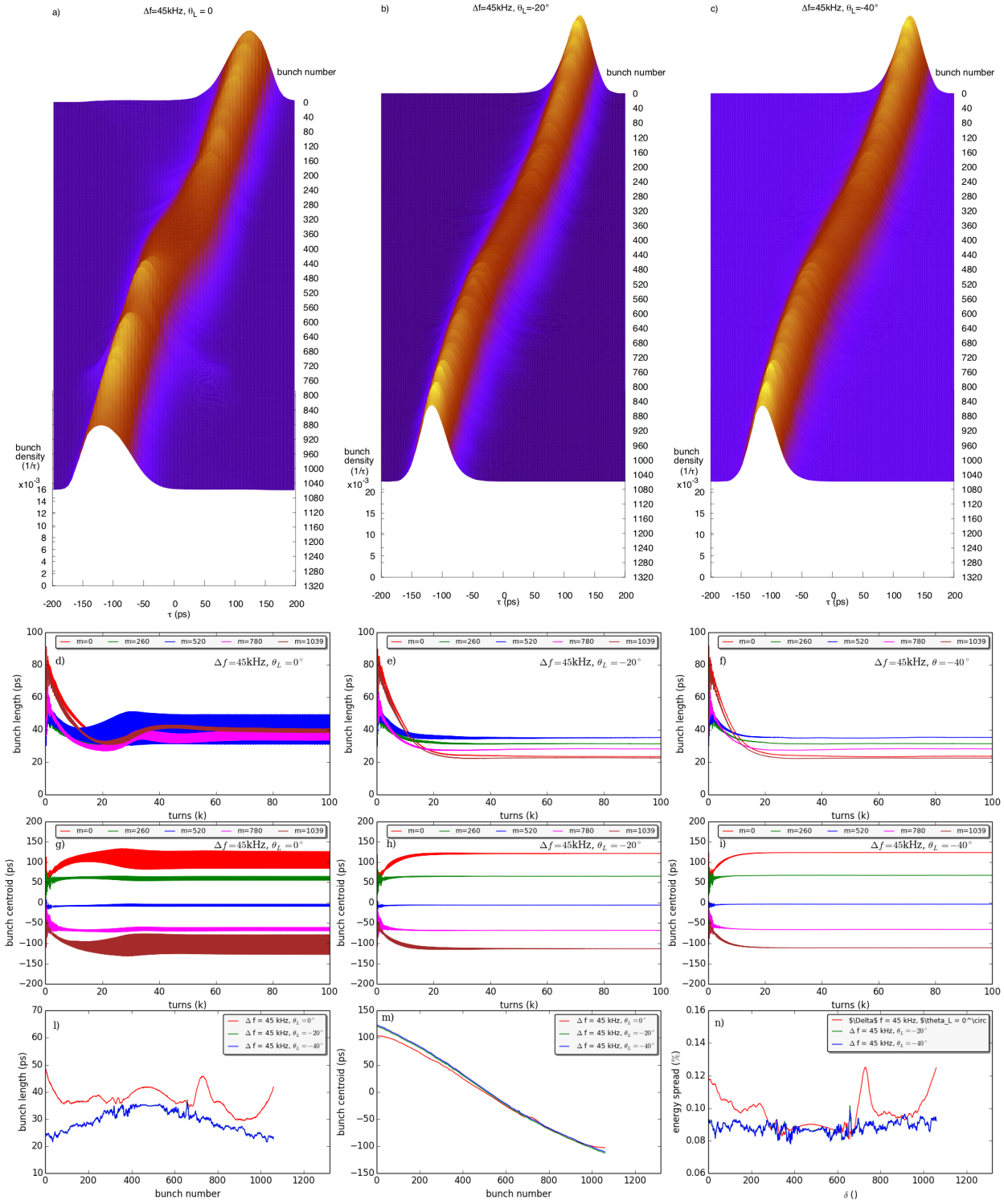

Figure 7: Numerical simulations up to $100,000$ turns with nominal gap, $g = 260$, and $\Delta f = 45$kHz, for load angle $\theta_L = 0$, $\theta_L = -20°$ and $\theta_L = -40°$. A stabilizing effect from a non zero load angle is seen for $\theta_L \in [-20°, 0°]$.

introduction of a non zero load is partially effective in stabilizing the HHC system, with the "stabilizing" load angle in the range $[-20°, 0°]$ for $\Delta f = 45$kHz, and $[-40°, -20°]$ for $\Delta f = 55$kHz.

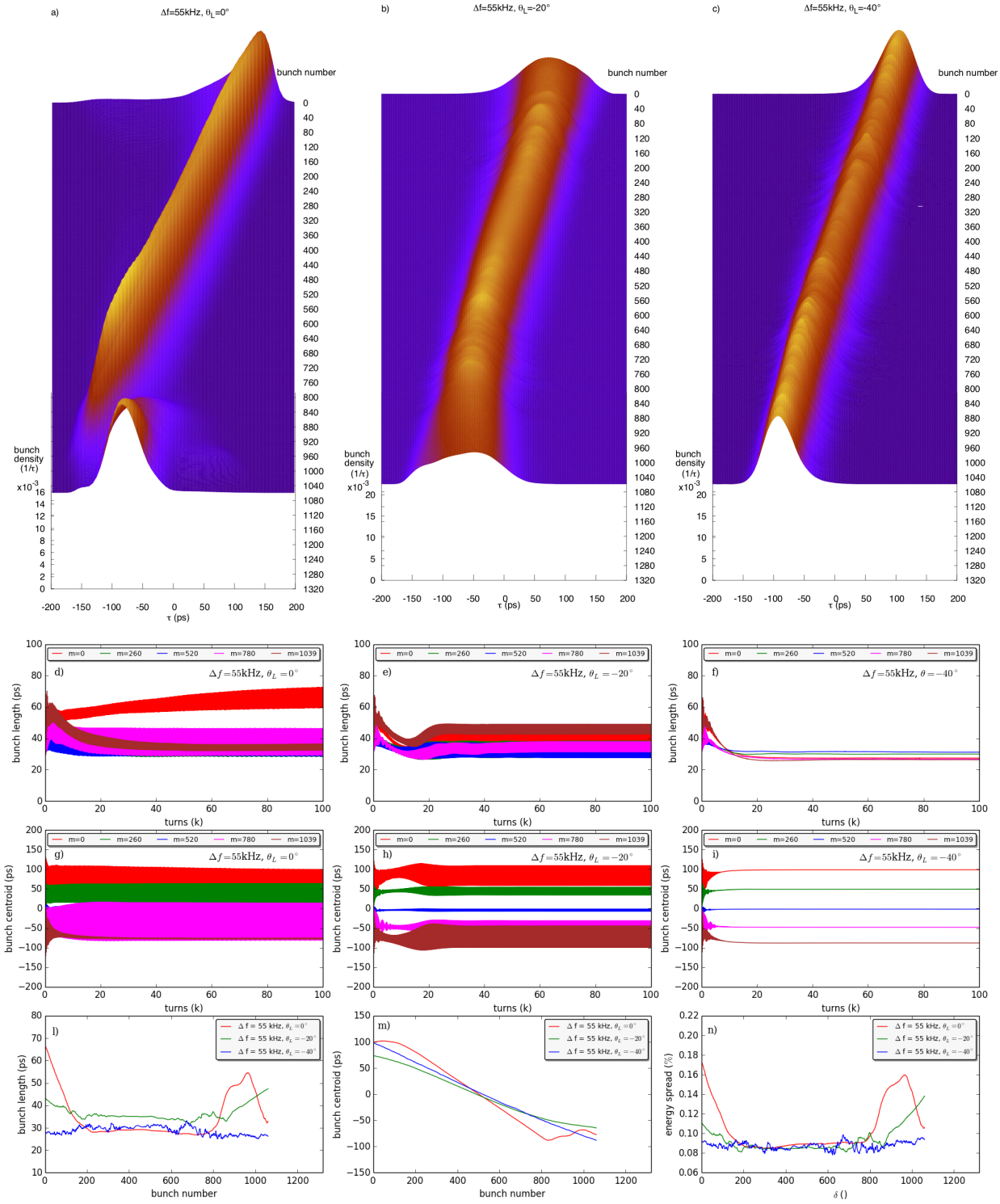

Figure 8: Numerical simulations up to 100,000 turns with nominal gap, $g = 260$, and $\Delta f = 55$kHz, for load angle $\theta_L = 0$, $\theta_L = -20°$ and $\theta_L = -40°$. The stabilizing effect from a non zero load angle is seen here for $\theta_L \in [-40°, -20°]$.

3 Conclusions

The numerical results discussed in Sec.2 clearly show a reduction in both performance and stability of the HHC system with the increase of the gap in the uniform filling, with the case of a gap $g = 130$,

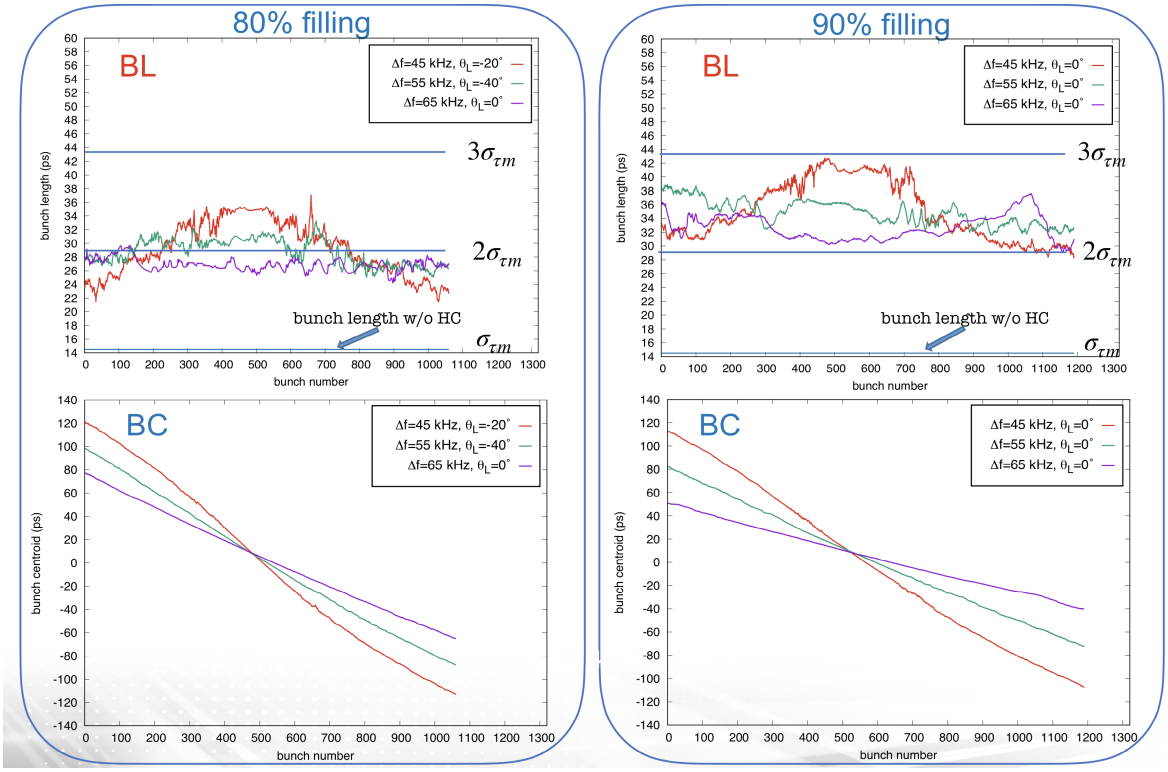

Figure 9: Performance of the HHC stable settings as a function of the detuning frequency Δf and load angle θ_L for $g = 260$ (80% fractional filling) and $g = 130$ (90% fractional filling). The bunch length and bunch centroid are labeled with BL and BC respectively.

corresponding to a 90% fractional filling, stable at all the detuning frequencies considered. On the other hand, the nominal case with $g = 260$, corresponding to a 80% fractional filling, has shown to be unstable for some values of the detuning frequencies. Moreover, the case with $g = 130$ has shown a superior performance in terms of bunch lengthening with respect to the nominal case. The performance of stable HHC settings for the nominal case $g = 260$ and the case $g = 130$, as a function of detuning frequency Δf and load angle θ_L, is shown in Fig.9, both in terms of average bunch lengthening and uniformity of the bunch centroid and bunch length across the train. For the nominal case $g = 260$, the numerical result with $\Delta f = 55$kHz and $\theta_L = -40\circ$ is included in the discussion for the sake of completeness, but should be excluded as possible operating point, since its large load angle would increase beyond acceptable limits the generator power. The top panels in Fig. 9 show that average bunch lengthening factor for the 80% and 90% fractional filling is approximately 2 and 2.5 respectively, to be compared with the bunch lengthening factor of the uniform filling case, which, according to Fig.4l, is approximately 3.5 for $\Delta f = 55$kHz. The performance reduction in the average bunch lengthening due to a gap in the uniform filling is therefore 45% for $g = 260$ and 30% for $g = 130$. Machine studies are planned at the NSLS-II storage ring to revisit the need of the nominal 80% fractional filling pattern for ion clearing, with the goal to increase the fractional filling towards a more uniform filling pattern. Arbitrary, more general multibunch configurations, such as filling patterns with multiple, smaller gaps than the nominal, are also under consideration. To this end, an analytical calculation to determine the beam loading voltage induced by arbitrary, stationary bunches has been done and implemented in a numerical code for fast parametric scans and guidance in Vlasov-Fokker-Planck simulations of the HHC system [22].

Appendix

Forcing the Equilibrium by Decreasing the Radiation Damping Time

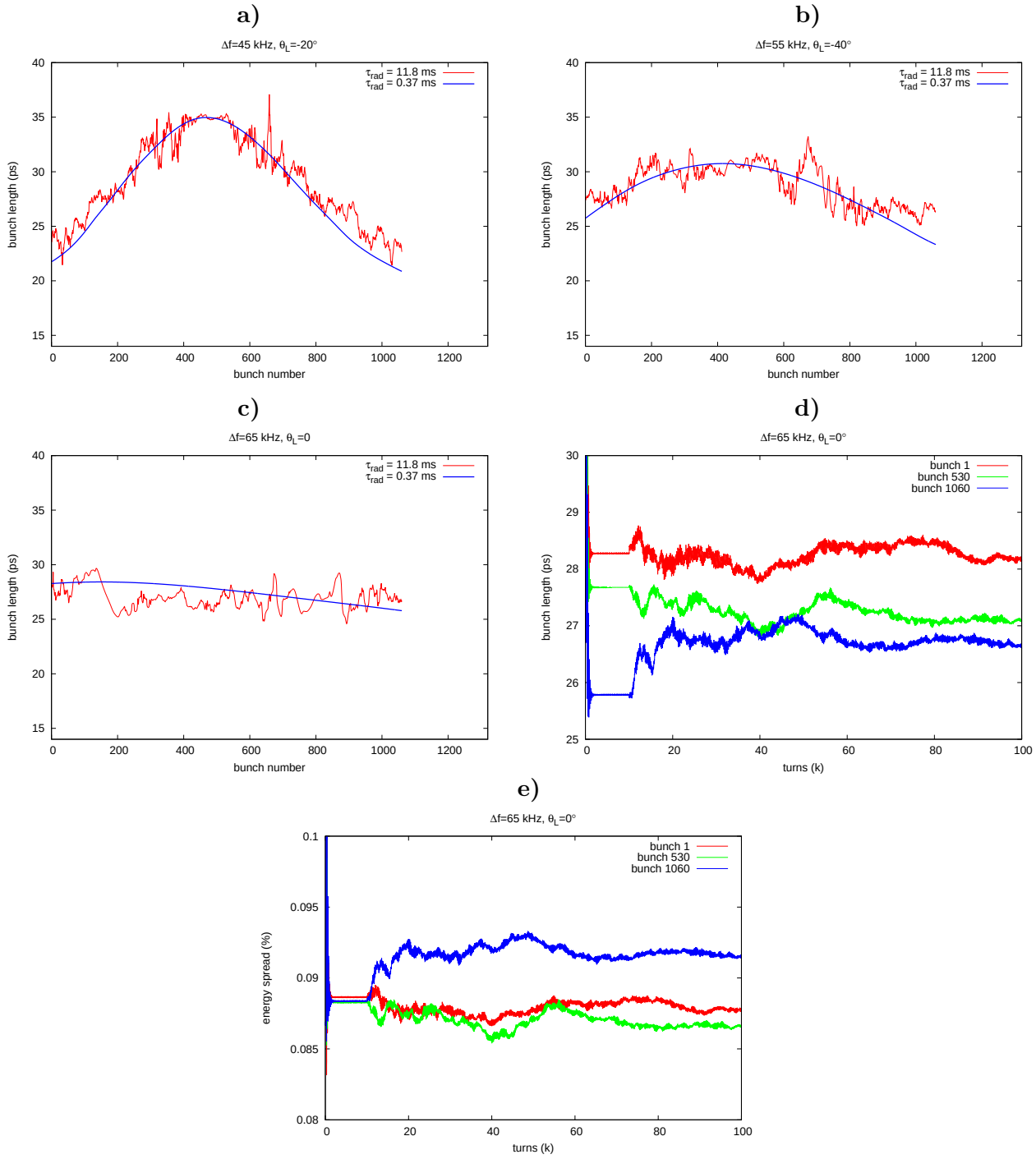

Figure 10: Comparison of the bunch length across the train for the case $g = 260$ with the nominal radiation damping $\tau_{\rm rad} = 11.8$ms (red trace) and with $\tau_{\rm rad} = 0.37$ms (blue trace), for the 3 cases discussed in Fig. 9: a) $\Delta f = 45$kHz and $\theta_L = -20°$, b) $\Delta f = 55$kHz $\theta_L = -40°$, c) $\Delta f = 65$kHz and $\theta_L = 0°$. d) Time evolution of the bunch length of bunch 1, 530 and 1060, with parameters of c), obtained by setting $\tau_{\rm rad} = 0.37$ms up to $10,000$ turns, and by restoring it to the nominal value $\tau_{\rm rad} = 11.8$ms afterwords. e) The same of d) for the energy spread.

The apparent fluctuations displayed by the bunch length across the train, as clearly shown in Fig. 9, have been studied by forcing the equilibrium artificially, in order to determined if the "fluctuating" behavior was induced by numerical noise in the simulations. Fig.10 shows the results of such a study, where the equilibrium has been forced by artificially decreasing the radiation damping from its nominal value $\tau_{\rm rad} = 11.8$ms to $\tau_{\rm rad} = 0.37$ms. Fig. 10a, b and c show the comparison after $100,000$ turns, while Fig. 10d and Fig. 10e show simulations where for the first $10,000$ turns the radiation damping has been set to $\tau_{\rm rad} = 0.37$ms, and then restored to its nominal vale . The apparent "fluctuating" behavior of the bunch length, displayed by energy spread as well, has been observed to be numerically reproducible and deterministic in nature, a behavior that can be the reflection of a state only marginally stable.

References

[1] G. Bassi, A. Blednykh and V. Smaluk, Phys Rev. Accel. Beams **19**, 024401 (2016).

[2] NSLS-II Conceptual Design Report (2006).

[3] A. Blednykh et al., paper MPPP037, Proceedings of PAC05 (2005).

[4] N. Towne, NSLS-II Technical Note **18** (2006); N. Towne, NSLS-II Technical Note **19** (2006); N. Towne, NSLS-II Technical Note **27** (2007); N. Towne, NSLS-II Technical Note **37** (2007).

[5] J. Rose et al., paper TUP055, Proceedings of PAC11, New York (2011).

[6] G. Penco and M. Svandrlik, Phys Rev. ST Accel. Beams **9**, 044401 (2006).

[7] M. Predozzi et al., paper MOP25, Proceedings of the 11th Workshop on RF Superconductivity, Lübeck/Travemünder, Germany (2003).

[8] G. Penco, Ph.D. thesis, Sincrotrone Trieste - University of Milan (2004).

[9] R. A. Bosh, K. J. Kleman, and J. J. Bisognano, Phys Rev. ST Accel. Beams **4**, 074401 (2001); R. A. Bosh Phys Rev. ST Accel. Beams **8**, 084401 (2005).

[10] G. Bassi, A. Blednykh and V. Smaluk, Phys Rev. Accel. Beams **19**, 024401 (2016).

[11] T. Olsson, *Timing Modes for the MAX IV Storage Rings*, Lund University, Faculty of Science, MAX IV Laboratory, 2018.

[12] P. F. Tavares, Å. Andersson, A. Hansson and J. Breunlin, Phys. Rev. ST Accel. Beams, **17**, 064401 (2014).

[13] A. Hofmann and Myers., Proceedings of the 11th International Conference on High Energy Accelerators, Geneva, 1980.

[14] NERSC, `http://www.nersc.org`.

[15] K.Y. Ng, *Physics of Intensity Dependent Beam Instabilities*, World Scientific Publishing, Singapore (2006).

[16] G. Bassi et al., paper TUPPP042, Proceedings of IPAC12, New Orleans, USA.

[17] F. J. Cullinan, R. Nagaoka, G. Skripka, and P. F. Tavares, Phys. Rev. Accel. Beams 19, 124401 (2016).

[18] M. Venturini, Phys. Rev. Accel. Beams 21, 024402 (2018).

[19] S. Krinsky and J. M. Wang, Particle Accelerators, Vol. 17, pp. 109-139, (1985).

[20] J.M. Byrd, S. De Santis, J. Jacob, and V. Serriere, Phys Rev. ST Accel. Beams **5**, 092001 (2002).

[21] J. Tagger and G. Bassi, NSLS-II Technical Note **287**, 2018.

[22] G. Bassi and J. Tagger, in preparation.